Earth, Planets and Space

FULL PAPER

Open Access

# El Niño–Southern Oscillation effect on ionospheric tidal/SPW amplitude in 2007–2015 FORMOSAT-3/COSMIC observations

Yang-Yi Sun[1*], Huixin Liu[1], Yasunobu Miyoshi[1], Loren C. Chang[2,3] and Libo Liu[4,5]

**Abstract**

This study examines the influence of the El Niño–Southern Oscillation (ENSO) on the ionospheric total electron content (TEC) diurnal eastward 3 (DE3) and stationary planetary wave 4 (SPW4) which are the major components of the ionospheric wave-4 longitudinal structure. The TEC is the integration of electron density from 200 to 800 km sounded by the GPS radio occultation experiment onboard the FORMOSAT-3/COSMIC satellites during the period of January 2007–December 2015. The results show that the TEC DE3 and SPW4 amplitudes respond to the ENSO signature in the thermospheric wind DE3 in the Northern Hemisphere during the lower-solar-activity period. The contribution of the ENSO cold phase in 2010 and 2011 to the quasi-biennial oscillation in the TEC DE3 and SPW4 amplitudes is not negligible.

**Keywords:** El Niño–Southern Oscillation, Ionospheric tide/SPW, Quasi-biennial oscillation, Radio occultation

## Introduction

Ionospheric plasma density structures are highly variable on broad range of temporal and spatial scales, and the solar activity and lower atmosphere forcing are the major drivers. The El Niño–Southern Oscillation (ENSO) ocean–atmosphere coupling phenomenon is one of the significant sources of variability in the thermosphere (Gurubaran et al. 2005; Lieberman et al. 2007; Pedatella and Liu 2012, 2013; Warner and Oberheide 2014; Liu 2016; Liu et al. 2017; Sun et al. 2018). However, studies on the ENSO signature in the ionosphere are rare and challenging (Pedatella and Forbes 2009; Pedatella and Liu 2013; Chang et al. 2018) due to the complex nature of the atmosphere–ionosphere-solar system. Pedatella and Liu (2013) simulated the influence of the ENSO-driven tidal variability on the low-latitude ionosphere. The simulations show that the interannual tidal variability in the mesosphere and lower thermosphere (MLT) can introduce 10–15% variability in the $\boldsymbol{E}\times\boldsymbol{B}$ vertical drift velocity and ionosphere peak density. Chang et al. (2018) analyzed the FORMOSAT-3/COSMIC (F3/C) S4 index from 2007 to 2014 and showed that ENSO signatures can transmit to *Es* formation mechanisms, potentially through modulation of vertically propagating atmospheric tides that alter lower thermospheric wind shears.

The ENSO-related variation in diurnal tides in the MLT (Gurubaran et al. 2005; Lieberman et al. 2007; Pedatella and Liu 2012, 2013; Warner and Oberheide 2014; Liu et al. 2017; Sun et al. 2018) can modulate the ionospheric wind dynamo which drives the equatorial ionospheric anomaly (EIA) wave-4 longitudinal structure on both sides of the magnetic equator via the fountain effect (Lühr et al. 2007; Wan et al. 2010; Fang et al. 2013). The diurnal eastward wavenumber 3 (DE3) and stationary planetary wavenumber 4 (SPW4) in the ionospheric electron density comprise the largest portion of the wave-4 structure (Pancheva and Mukhtarov 2012; Chang et al. 2013, 2016). Therefore, this study analyzes the total electron content (TEC) of F3/C to explore the ENSO effect on the ionospheric DE3 and SPW4 amplitudes from January 2007 to December 2015. The period comprises two ENSO warm (2009/2010, 2014/2015)/cold (2007/2008, 2010/2011) phases. The rest of the periods are weak ENSO phases and neutral conditions (according to the Ocean Niño Index, http://www.cpc.ncep.noaa.gov/products/analysis_monitoring/ensostuff/ensoyears.shtml).

*Correspondence: yysun0715@gmail.com
[1] Department of Earth and Planetary Science, Kyushu University, Fukuoka 819-0395, Japan
Full list of author information is available at the end of the article

Warner and Oberheide (2014) reported the notable increases in the wind DE3 amplitude in the lower thermosphere within the 0°–20°N latitude band during the ENSO cold phase (2007/2008 and 2010/2011). Especially during the 2010/2011 strong ENSO cold phase, enhanced forcing from below during the winter months causes a ~70% increase in the zonal wind DE3 tide in the MLT region. They also suggested that constructive interference of the antisymmetric and symmetric tidal contributions results in the larger MLT zonal wind DE3 amplitude in the Northern Hemisphere during the strong La Niña. Accordingly, this study also conducts the zonal wind DE3 amplitude observed by Thermosphere Ionosphere Mesosphere Energetics and Dynamics (TIMED)/TIMED Doppler Interferometer (TIDI) at 100 km altitude to suggest a causal mechanism for the ionospheric tide/SPW response to the ENSO phases. Note that the ionospheric diurnal westward wavenumber 1 (DW1) primarily reflects in situ photoionization that produces ionization peaks. The numerical experiments by Hagan et al. (2001) suggested that the MLT DW1 cannot vertically propagate above 130 km altitude. Comparing the TEC DW1 with the other components is helpful to recognize the TEC tide/SPW response to the ENSO-related variation from the lower thermosphere.

Moreover, the quasi-biennial oscillation (QBO) is an important and persistent feature in the thermosphere and ionosphere. The ENSO can modulate the stratospheric QBO (Taguchi 2010) as well as the QBO components in the temperature DW1 and DE3 in the MLT (Sun et al. 2018). Both the wind DE3 in the lower thermosphere and solar activity can affect the QBO in the TEC tidal/SPW amplitudes (Chang et al. 2016; Wang et al. 2018). However, it is challenging to distinguish the ionospheric QBO response to the stratospheric QBO and the QBO component in solar activity because they yield similar periodicities (Tang et al. 2014). Accordingly, we examine whether the ENSO is capable of influencing the QBO in the ionospheric tide/SPW.

## Data and methodology

The Global Positioning System (GPS) radio occultation (RO) experiment onboard the F3/C satellites observed ionospheric electron density (from 70 to 800 km altitude) for over 10 years since their launch in 2006. The F3/C mission consists of six microsatellites in the different mission planes and provides observations of vertical structures of the ionospheric electron density globally by using the radio occultation observation technique. The electron density profiles from F3/C have significantly improved our understanding of the global morphology and variability of the dynamical EIA structures (Lin et al. 2007, 2012; Maruyama et al. 2016). The F3/C electron density profiles are adopted from the ionPrf file in the second data level which is processed by the COSMIC Data Analysis and Archive Center (http://cosmic-io.cosmic.ucar.edu/cdaac/index.html) using the Abel inversion technique from TEC along LEO (low earth orbit)—GPS rays since May 2006. Yue et al. (2010) and Liu et al. (2010) reported that the electron density profiles obtained by the Abel inversion have large amount of error below 200 km altitude. The F3/C TEC used in this study is the integration of electron density from 200 km to the LEO satellite altitude (800 km). The global TEC observation of F3/C RO with uniformly spatial and temporal distributions from 2007 to 2015 is essential for properly resolving the tidal/SPW components with higher longitudinal wavenumber. The sounding rate of the F3/C RO is low after 2015.

The zonal wind in the lower thermosphere was obtained by the Thermosphere Ionosphere Mesosphere Energetics and Dynamics (TIMED)/TIMED Doppler Interferometer (TIDI) from January 2007 to December 2015 (http://download.hao.ucar.edu/archive/tidi/data/vec0307a/). The TIDI wind observation is successfully utilized in studying migrating and non-migrating tides in the MLT (Wu et al. 2008a, b).

The F3/C TEC and TIDI wind data are binned into 5° latitude for the tidal computation. The absolute tidal amplitudes are fitted from the values at each latitude grid using the linear least-squares method (Wu et al. 1995) with the following basis function:

$$F(\lambda,t) = \bar{F} + \sum_{n=1}^{3}\sum_{s=-4}^{4} \hat{F}_{n,s}\cos\left(n\Omega t - s\lambda - \hat{\psi}_{n,s}\right) + \sum_{s=1}^{4} \hat{F}_{s}\cos\left(s\lambda - \hat{\psi}_{s}\right), \quad (1)$$

in which $\hat{F}$ and $\hat{\psi}$ are tidal amplitude and phase. $\bar{F}$ is the zonal mean value. $n$ and $s$ are the tidal harmonic from 1 to 3 (diurnal, semidiurnal, terdiurnal) and zonal wave number from $-4$ to 4 (westward negative). $\Omega = \frac{2\pi}{24}h^{-1}$, $\lambda$ and t are longitude and universal time, respectively. The tides from F3/C and TIDI are estimated, respectively, from the data collected with the 45-day and 60-day windows, which moved monthly through the period from 2007 to 2015. The wavelet analysis (Torrence and Compo 1998) is applied to show an overall feature of the temporal variation in the tidal amplitudes on various scales.

## Result

The left panels of Fig. 1 show that the amplitudes of the F3/C TEC DW1, DE3, and SPW4 are intense within the ±30°N geomagnetic latitude. The amplitude anomaly as shown in the right panels is defined as by subtracting the mean annual cycle from the detrended time series of tidal/SPW amplitude at each latitude. We have applied a

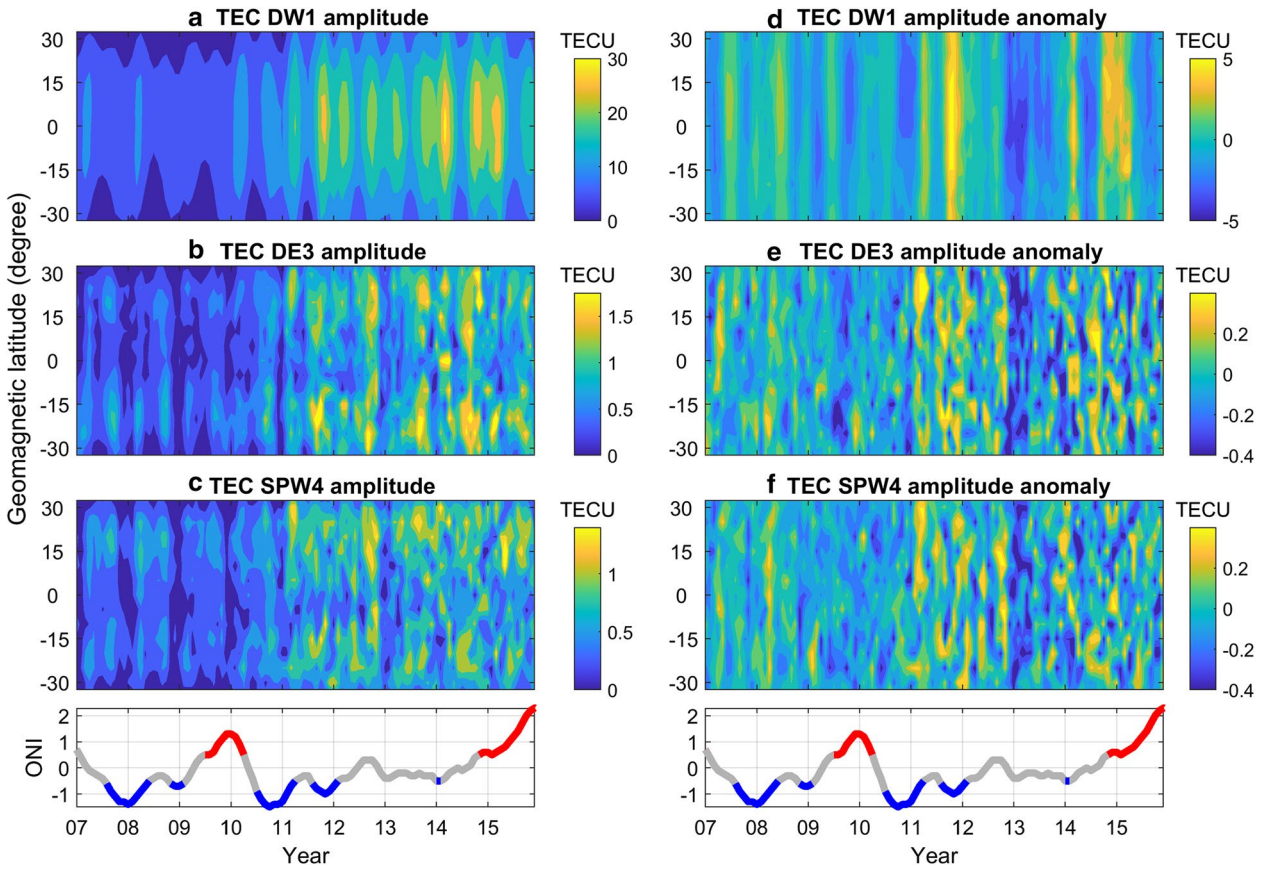


**Fig. 1** (Left) Amplitude of the F3/C TEC (top row) diurnal westward wavenumber 1 (DW1), (second row) diurnal eastward wavenumber 3 (DE3), and (third row) stationary planetary wavenumber 4 (SPW4) as a function of time and geomagnetic latitude. The latitudinal and temporal resolutions are 5° and 1 month, respectively. (Right) Amplitude anomalies as a function of geomagnetic latitude. The anomaly is defined as by removing the mean annual variation from the detrended time series of tidal/SPW amplitude at each latitude. The bottom panel is the Oceanic Niño Index (ONI). Red and blue (exceeding the threshold of ± 0.5 °C) on the ONI indicate the ENSO (El Niño–Southern Oscillation) warm and cold phases

polynomial regression (Matlab polyfit) with order from 1 to 5 to fit the trend of the TEC tidal/SPW amplitudes. The fitting trends from third to fifth order are nearly identical and represent the tendency of the solar cycle (not show). Therefore, the third-order polynomial regression is performed on the time series to fit the trend. The mean annual cycle is the average of the 10-year detrended time series. The amplitude anomalies being stronger/weaker in the higher-/lower-solar-activity periods suggest the solar activity disturbing the TEC tidal/SPW amplitudes. The TEC tidal/SPW amplitude anomalies do not show obvious hemispheric symmetry (right panels). The TEC DE3 and SPW4 amplitudes can be also driven by the wind DE3 in the lower thermosphere that contains significant asymmetric pattern (Oberheide and Forbes 2008) that could result in different amplitude variations in the Northern and Southern Hemispheres. Accordingly, the amplitude anomalies are averaged within 0° to 30°N (Northern Hemisphere) and 0° to 30°S (Southern Hemisphere) for the further wavelet analysis. No obvious agreement between the ENSO variability (Oceanic Niño Index, ONI) and the TEC DE3 and SPW4 amplitudes is shown in Fig. 1.

Figure 2 shows the wavelet analysis for the time series of the TEC tidal/SPW amplitude anomalies in the Northern (top panels) and Southern (bottom panels) Hemispheres. All the wavelet spectra show intense signals with periods ranging from ~ 1.5 to 4 years that relates to the QBO signals from the lower atmosphere and solar activity (Chang et al. 2016). The signals with shorter periods (from several months to ~ 1 year) are pronounced mainly in the higher solar activity period from 2011 to 2015. The left panels show that, in the Northern Hemisphere, the TEC DW1 exhibits spectral peaks with period of ~ 0.6 years maximizing in middle 2011 and with period of ~ 1 year from 2008 to 2010 and from 2014 to 2015. In the Southern Hemisphere, the spectral peaks with periods of ~ 0.6 years and ~ 0.5–1 years maximizing in middle 2011

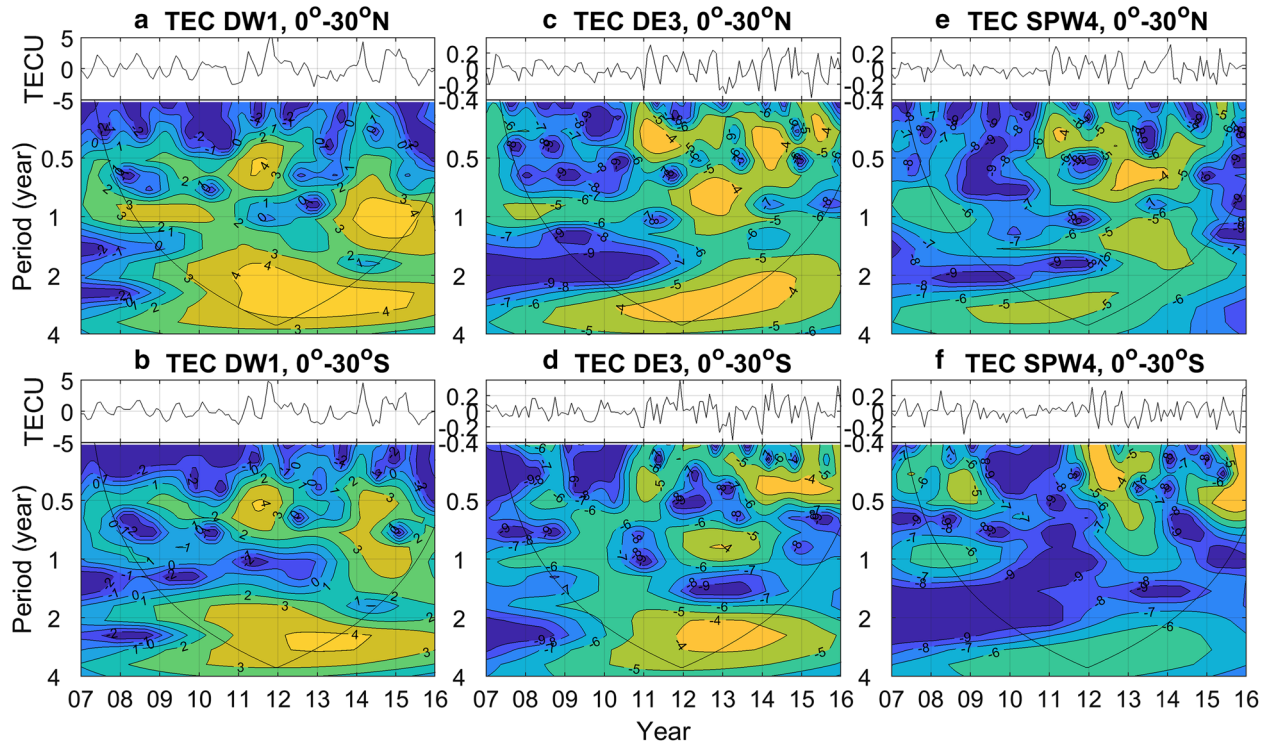


**Fig. 2** Wavelet power spectra of **a**, **b** the TEC DW1, **c**, **d** DE3, and **e**, **f** SPW4 amplitude anomalies averaged within the latitude of **a**, **c**, **e** 0° to 30°N and **b**, **d**, **f** 0° to 30°S. Black curves indicate the cone of influence zone of the wavelet analysis. The panels above the spectra show the amplitude anomalies

and with periods of ~0.5–1 years in 2014. In the middle panels, the TEC DE3 has spectral peaks with period of ~0.3 years maximizing in early 2011, 2014, and 2015 and with periods of ~0.7–1 years in 2012 in the Northern Hemisphere. The peak with period of ~0.3 years maximizes in early 2011 in the Southern Hemisphere, but its magnitude is much weaker than that in the Northern Hemisphere. In the right panels, the spectral peaks of the TEC SPW4 in the Northern Hemisphere with period of ~0.3 years maximize in early 2011 and with periods of ~0.5–0.8 years maximize from 2012 to 2013. In the Southern Hemisphere, peaks with period shorter than 0.5 years appear in 2012 and 2015. There is no peak with period of ~0.3 years in 2011.

Figure 3 shows the wavelet spectra of the 10.7 index and the wind DE3 in the lower thermosphere, which are the major drivers for the changes of the TEC tide/SPW. In Fig. 3a, the F10.7 spectrum shows the spectral peak with periods ranging from 2 to 4 years after 2011. The peak with periods of ~0.5–1 years maximize in 2011 and 2014. The solar cycle 24 ascends in 2011. The solar activity is high during 2014/2015. The good agreement between the spectra of the TEC DW1 and F10.7 confirm that the TEC DW1 is highly controlled by the solar activity. On the other hand, Fig. 3b and c shows the spectra of the amplitude anomaly of the TIMED/TIDI-observed zonal wind DE3 at 100 km altitude in both the two Hemispheres from 2007 to 2015. Figure 3b shows that, in the Northern Hemisphere, the spectral peaks with periods of ~0.5–1.5 years maximize mainly from 2010 to 2012. The peak with periods of ~2–3 years is intense from 2007 to 2012. The peak intensity in the Southern Hemisphere is weaker than that in the Northern Hemisphere (Fig. 3c).

The spectral peaks of the wind DE3 and F10.7 are distributed mainly within the period intervals of 0–12 months, 12–24 months, and 24–48 months (Fig. 3). However, the distribution of the spectral peaks of the TEC tidal/SPW amplitudes are rather complicated (Fig. 2). To better resolve the ENSO signature in the TEC tide/SPW, the time series of the TEC tidal/SPW and wind DE3 amplitude anomalies as well as the F10.7 index are divided into the components with the three period intervals using a band-pass filter and further compared with each other (Fig. 4).

In the left panels of Fig. 4, the components with the period interval of 0–12 months are highly fluctuating through the entire period from 2007 to 2015. It is difficult to glean the ENSO signature from the

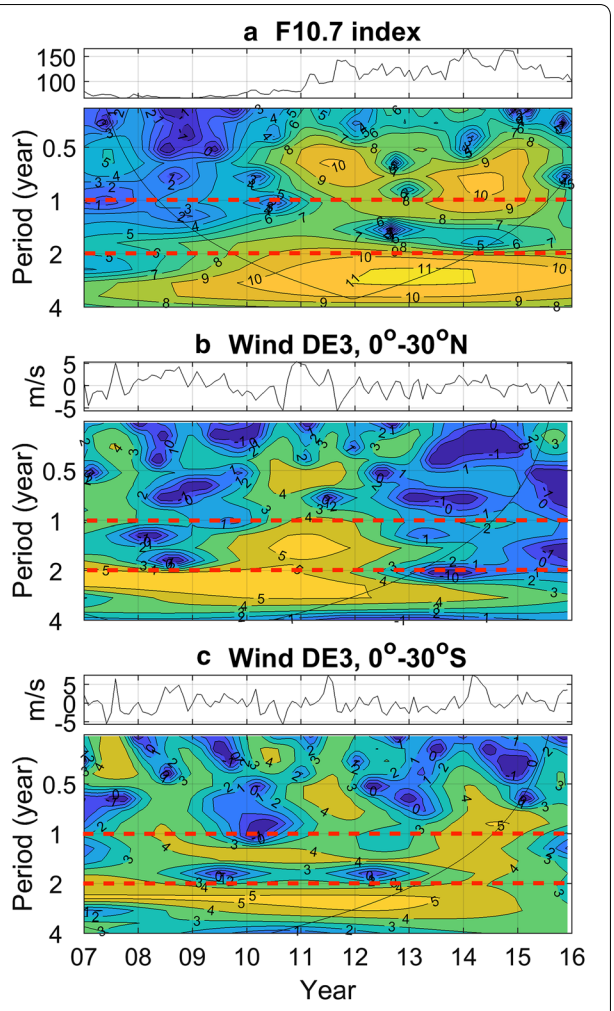


**Fig. 3** Wavelet spectra of **a** the F10.7 index, and TIDI zonal wind DE3 amplitude anomalies in **b** the Northern and **c** Southern Hemispheres. The dash lines divide the spectra into three period intervals of 0–12 months, 12–24 months, and 24–48 months

short-period components (0–12-month period band) because they are highly fluctuated. The middle panels show that the components of the TEC DW1 and F10.7 with the period interval of 12–24 months agree well from 2011 to 2015 (higher solar activity period). The components of DW1 and F10.7 are out of phase to the wind DE3 near the 2010–2011 winter. It is due to the fact that the TEC DW1 is highly controlled by the solar activity. The wind DE3 in the lower thermosphere cannot control the DW1 but can induce a DE3 variation in TEC. The wind DE3 increases significantly near the 2010–2011 winter, the components of the wind DE3 and TEC DE3/SPW4 show good agreement during the 2010/2011 ENSO cold phase when the crests of the TEC DE3/SPW4 and wind DE3 are closer to each other. There is a difference of few months between the crests of the wind DE3 and TEC DE3/SPW4. The right panels show the comparison of the components with the period interval of 24–48 months. It is not surprising to see the good agreement between the long-term variation in the TEC DW1 amplitude anomaly and F10.7. On the other hand, it is hard to distinguish the effect of solar activity and wind DE3 on the long-term variation in the TEC DE3 and SPW4, because the few cycles yield similar periodicities and are nearly in phase with each other. In the Southern Hemisphere, the TEC DW1 and F10.7 agree well with each other in varies scales especially during the higher solar activity period. It is difficult to indicate the connection between the TEC DE3/SPW4 and MLT wind DE3 components with period intervals of 12–24 months and 24–48 months due to the contamination of solar activity and the weaker wind DE3 in the Southern Hemisphere (Fig. 3c). We do not show the results for the Southern Hemisphere because the amplitude anomalies with period longer than 1 year are weaker there.

The spectra of the wind DE3 and F10.7, respectively, show the prominent signals with periods of ~1.5–3 years and 2–4 years (Fig. 3) which involve signals with the QBO scale (period of ~28 month). In Fig. 5, a band-pass filter with cutoff period ranging from 18 to 34 months (Xu et al. 2009) is applied to extract the QBO component from the F10.7 index and the amplitude anomalies of the TEC tidal/SPW and wind DE3 in the Northern Hemisphere. Note that no obvious agreement exists between the anomalies of the TEC DE3/SPW4 and wind DE3 in the Southern Hemisphere due to the weaker amplitude there (not shown). In Fig. 5a, the QBO components of the DW1 amplitude anomaly and F10.7 are almost identical through the entire period from 2007 to 2015. The QBO crests of the TEC DW1 and F10.7 are out of phase with the wind DE3 during the 2010/2011 ENSO cold phase. In Fig. 5b, The QBO components of the TEC DE3 and F10.7 have a good agreement during the higher solar activity period from 2012 to 2015. In the lower-solar-activity period of 2007–2011, the QBO crests of the TEC DE3 and wind DE3 are closer in 2008 and the winter of 2010/2011. In Fig. 5c, the QBO components of TEC SPW4 and wind DE3 agree well with each other from 2007 to 2011. Their QBO crests are almost in phase near the winter of 2010/2011. There is a slight phase shift between the TEC SPW4 and wind DE3 QBO signals. The shift between the TEC DE3/SPW4 and the MLT wind DE3 during the ENSO phases should be considered in future studies.

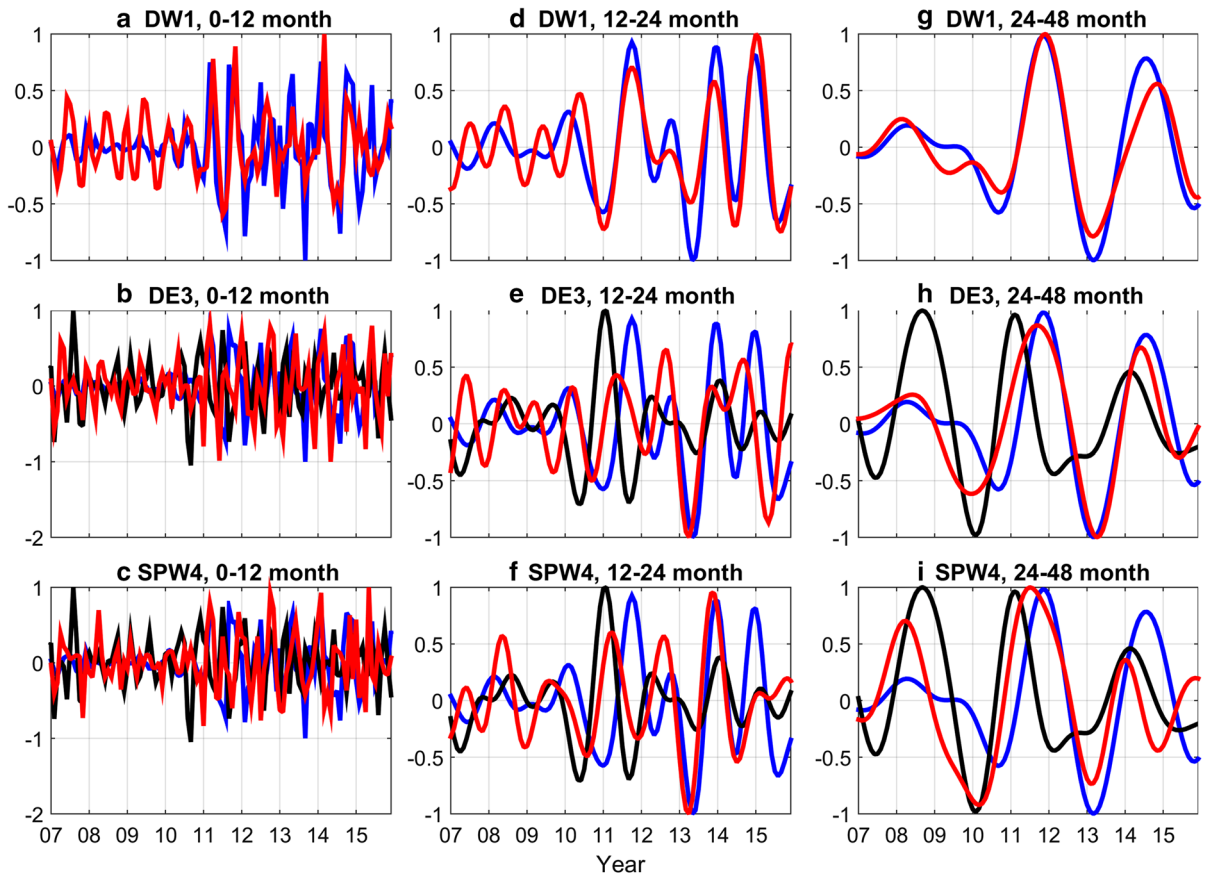


**Fig. 4** Comparison of the components of **a**, **d**, **g** the TEC DW1, **b**, **e**, **h** DE3, and **c**, **f**, **i** SPW4 (red curve) amplitude anomaly to the wind DE3 amplitude anomaly (black curve) and F10.7 (blue curve) with periods ranging from **a**, **b**, **c** 0–12 months, **d**, **e**, **f** 12–24 months, **g**, **h**, **i** 24–48 months in the Northern Hemisphere. The components have been normalized within ± 1 for the comparison. No obvious agreement between the anomalies of the TEC DE3/SPW4 and wind DE3 in the Southern Hemisphere due to the weaker amplitude there (not show)

## Discussion

The QBO components as shown in Fig. 5 agree with the QBOs decomposed from the TEC tidal/SPW amplitudes using the adaptive method named multi-dimensional ensemble empirical mode decomposition (Chang et al. 2016). Chang et al. (2016) reported that the TEC SPW4 and DE3 QBOs start increasing in middle 2010, but the DW1 and SW2 (semidiurnal westward 2) as well as the QBO component of F10.7 start increasing in early 2011. The band-pass filter applied in this study bases on the Fourier assumption, but the multi-dimensional ensemble empirical mode decomposition is an adaptive method without a basis function assumption. The results from the two independent methods agree with each other. The agreement reveals that, besides the effect of the solar radiation and ionosphere/thermosphere composition changes, the ENSO-related wind DE3 variation contributes to the QBO in the TEC DE3 and SPW4 during the strong 2010/2011 ENSO cold phase. The response of the wind DE3 in the lower thermosphere to the 2007/2008 ENSO cold phase is not as significant as that to the 2010/2011 ENSO cold phase (Warner and Oberheide 2014). It can be the reason of that the ionosphere response to the 2007/2008 ENSO cold phase is weak. Warner and Oberheide (2014) suggested that the ENSO-related enhanced forcing from below causes an increase in the zonal wind DE3 tide in the MLT region especially during the winter months of the 2010/2011 strong ENSO cold phase. Note that we have examined all the TEC tidal/SPW components with zonal wave number ranging from -4 to +4 and tidal harmonic from the diurnal to terdiurnal modes. The ENSO-related signature is most pronounced in the TEC DE3 and SPW4.

The stratospheric QBO can affect the diurnal tides in the lower thermosphere (Forbes et al. 2008; Oberheide et al. 2009) and ionosphere (Tang et al. 2014; Chang et al. 2016; Wang et al. 2018). The wind DE3 amplitude shows an intense peak with period shorter than 2 years during the 2010/2011 ENSO cold phase (Fig. 3b). However, the wavelet spectrum of the U30 index that stands for the

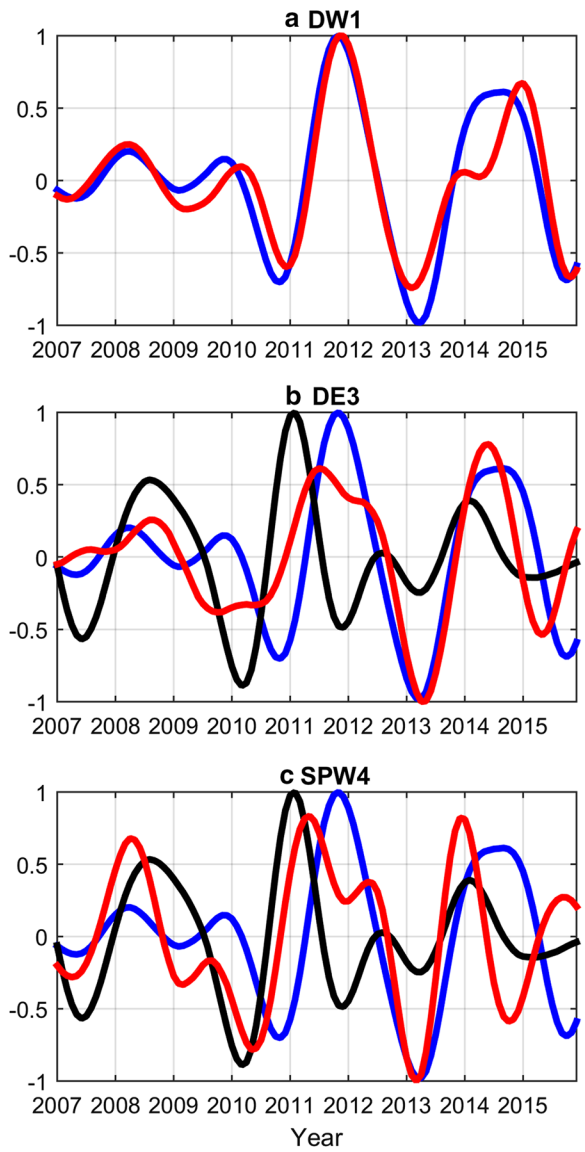


**Fig. 5** Comparison of the quasi-biennial oscillation (QBO) components of the amplitude anomalies of the TEC tidal/SPW (red curve) and zonal wind DE3 (black curve) in lower thermosphere, as well as the F10.7 index (blue curve). A band-pass filter with the cutoff period ranging from 18 to 34 months is applied to extract the QBO component from the time series. The QBO components have been normalized within ±1 for the comparison

stratospheric QBO does not show strong short-period signals during that period (Fig. 4 in Sun et al. 2018). Warner and Oberheide (2014) showed similar percent variations in DE3 heating and tidal wind deviations during the period of 2008–2011, indicating a strong ENSO influence, with a few exceptions that can be accounted for by the effects of the stratospheric QBO. Therefore, the QBO components of the TEC DE3 and SPW4 amplitudes are driven by the ENSO signature in the wind DE3, rather than the stratospheric QBO.

The series of ENSO warm phases shorten the QBO components in the zonal wind and temperature diurnal tides in the lower thermosphere from 2002 to 2007 (Sun et al. 2018). However, the individual ENSO warm phase of 2009/2010 may not allow us to show a robust TEC tidal/SPW response. This could be due to the negligible response of the wind DE3 during the ENSO warm phase (Warner and Oberheide 2014). Different types of ENSO warm phases, which are usually based on the location of the largest positive sea surface temperature anomalies, can result in different effects on the atmosphere (Johnson 2013).

The 2014/2015 ENSO warm phase is strong but occurs in the high-solar-activity period. The ENSO would impact ionosphere during the entire F3/C operational period, but the high solar activity contaminates the ENSO effect from the lower atmosphere. The neutral DE3 coupling into the ionosphere via the E-region dynamo can be modulated by the DW1 component of the conductivities and produce the SPW4 in electron density (Chang et al. 2013). The dynamo-driven ionospheric tidal/SPW is sensitive to the solar activity because the conductivities are highly dependent on the solar irradiance variation. Therefore, the contamination of solar activity can obscure the ENSO signature in the ionospheric tidal/SPW if the ENSO effect transmits into the ionosphere via the dynamo process. Longer data sets including numerous ENSO warm phases under low-solar activity conditions are required for studying the ionospheric tidal/SPW response to the ENSO warm phase.

The stratospheric QBO period is flexible and its mean period is near 28 months. However, the peak in the longer periods occurs close to 36 months in the solar activity that can border the QBO period range (18–34 months) of the ionospheric tide/SPW. The peaks of F10.7 and wind DE3 in the period near 1.5 years in 2010–2011 can also shorten the ionospheric QBO. The impact from the solar activity results in the period of the ionospheric QBO is more flexible than that of the QBO in the lower atmosphere.

On the short-period scales, the good agreement between the spectra of the F10.7 index (Fig. 3a) and the TEC DW1 amplitude anomalies (Fig. 2a, b) suggests that the solar activity induces the spectral peaks of the TEC DW1 with a period of ~0.6 years in both hemispheres in middle 2011. On the other hand, the spectral peaks of the TEC DE3 and SPW4 amplitude anomalies with period of ~0.3 years in early 2011 (Fig. 2c, e) may reflect the notable spectral peak of the wind DE3 amplitude anomaly with shorter periods in the Northern Hemisphere during the 2010/2011 ENSO cold phase (Fig. 3b). The spectral

peak of the TEC DE3/SPW4 leads that of the F10.7 by nearly a half year. Therefore, the solar activity cannot induce the short-period signals of the TEC DE3/SPW4 amplitude in early 2011, but perturbs them in middle 2011.

Both the amplitude anomalies of the TEC DE3/SPW4 (Fig. 2c, e) and wind DE3 (Fig. 3a) strengthen in the Northern Hemisphere during the 2010/2011 ENSO cold phase. This reveals that some other causal mechanisms result in the anomalies appearing in the Northern Hemisphere besides the ionospheric dynamo, which drives the ionosphere in both hemispheres. Forbes et al. (2009) first showed that the upper thermospheric temperature DE3 represents the direct vertical propagation of non-migrating tides upward from the troposphere. Oberheide et al. (2009) applied a physics-based empirical fit model to connect the tides from TIMED satellite to the CHAMP satellite at 400 km. They found that the DE3 amplitudes in the upper thermosphere can increase by a factor of 3 in the zonal wind, by 60% in temperature and by a factor of 5 in density, caused by reduced dissipation above 120 km during solar minimum. It is therefore possible that the ENSO signature in the MLT neutral DE3 (Warner and Oberheide 2014) is capable of transmitting into the *F* region altitude in the Northern Hemisphere. The nonlinear interaction between the DE3 and in situ generated DW1 in the neutral thermosphere can produce an SPW4 (Hagan et al. 2009; Pedatella et al. 2012). The ENSO signature in DE3 and SPW4 in the upper thermosphere could transmit to the ionosphere through ion drag.

## Conclusion

The ionospheric total electron content (TEC) diurnal eastward 3 (DE3) and stationary planetary wave 4 (SPW4) amplitudes measured by FORMOSAT-3/COSMIC respond to the ENSO signature in the lower thermophore during the lower-solar-activity period from 2007 to 2011. The 2010/2011 strong ENSO cold phase significantly enhances the TEC DE3 and SPW4 amplitudes with periods from 1 year to quasi-biennial periodicity at low latitude of the Northern Hemisphere. The QBO crests of the TEC DE3/SPW4 and the wind DE3 at lower thermosphere are almost in phase during the 2010/2011 ENSO cold phase. The solar activity dependence is hard to be entirely removed from the observation. Fixing the solar activity in the model simulation will enable extraction of ENSO signature uncontaminated by the solar activity.

#### Abbreviations

ENSO: El Niño–Southern Oscillation; TEC: total electron content; DE3: diurnal eastward wavenumber 3; SPW4: stationary planetary wavenumber 4; DW1: diurnal westward wavenumber 1; SW2: semidiurnal westward 2; MLT: mesosphere and lower thermosphere; EIA: equatorial ionospheric anomaly; F3/C: FORMOSAT-3/COSMIC; TIMED: Thermosphere Ionosphere Mesosphere Energetics and Dynamics; TIDI: TIMED Doppler Interferometer; QBO: quasi-biennial oscillation; GPS: Global Positioning System; RO: radio occultation; LEO: low earth orbit; ONI: Oceanic Niño Index.

#### Authors' contributions

YYS, HL, YM, LCC, and LBL designed and performed experiments. YYS analyzed data and drafted the manuscript. LCC developed the tidal fitting tool. All authors read and approved the final manuscript.

#### Author details

[1] Department of Earth and Planetary Science, Kyushu University, Fukuoka 819-0395, Japan. [2] Graduate Institute of Space Science, National Central University, Taoyuan 32001, Taiwan. [3] Center for Astronautical Physics and Engineering, National Central University, Taoyuan 32001, Taiwan. [4] Key Laboratory of Earth and Planetary Physics, Institute of Geology and Geophysics, Chinese Academy of Sciences, Beijing 100029, China. [5] Geoscience School, University of the Chinese Academy of Sciences, Beijing 100049, China.

#### Acknowledgements

Not applicable.

#### Competing interests

The authors declare that they have no competing interests.

#### Availability of data and materials

The FORMOSAT-3/COSMIC ionospheric electron density observation is downloaded from ftp://cdaac-ftp.cosmic.ucar.edu/. The TIMED/TIDI zonal wind observation is downloaded from http://download.hao.ucar.edu/archive/tidi/data/vec0307a/.

#### Consent for publication

Not applicable.

#### Ethics approval and consent to participate

Not applicable.

#### Funding

Y Y. S. was support by the NICT International Exchange Program. H. L. was support by JSPS KAKENHI grants 18H01270, 18H04446, and 17KK0095. Y. M. was supported by JSPS KAKENHI grant (B)15H03733. L. C. C. was supported by grants MOST 103-2111-M-008-019-MY3, 106-2111-M-008-010, and 107-2111-M-008-002-MY3 from the Taiwan Ministry of Science and Technology. L. B. L. was supported by National Natural Science Foundation of China (41621063).

## Publisher's Note



Received: 14 September 2018 Accepted: 25 February 2019
Published online: 27 March 2019

#### References

Chang LC, Lin CH, Yue J, Liu JY, Lin JT (2013) Stationary planetary wave and nonmigrating tidal signatures in ionospheric wave 3 and wave 4 variations in 2007–2011 FORMOSAT-3/COSMIC observations. J Geophys Res Space Phys 118:6651–6665. https://doi.org/10.1002/jgra.50583

Chang LC, Sun YY, Yue J, Wang JC, Chien SH (2016) Coherent seasonal, annual, and quasi-biennial variations in ionospheric tidal/SPW amplitudes. J Geophys Res Space Phys 121:6970–6985. https://doi.org/10.1002/2015JA022249

Chang LC, Chiu PY, Salinas CCJH, Chen SP, Duann Y, Liu JY, Lin CH, Sun YY (2018) On the relationship between E region scintillation and ENSO observed by FORMOSAT-3/COSMIC. J Geophys Res Space Phys 123:4053–4065. https://doi.org/10.1029/2018JA025299

Fang TW, Akmaev R, Fuller-Rowell T, Wu F, Maruyama N, Millward G (2013) Longitudinal and day-to-day variability in the ionosphere from lower atmosphere tidal forcing. Geophys Res Lett 40:2523–2528. https://doi.org/10.1002/grl.50550

Forbes JM, Zhang X, Palo S, Russell J, Mertens CJ, Mlynczak M (2008) Tidal variability in the ionospheric dynamo region. J Geophys Res Space Phys 113:A02310. https://doi.org/10.1029/2007JA012737

Forbes JM, Bruinsma SL, Zhang X, Oberheide J (2009) Surface-exosphere coupling due to thermal tides. Geophys Res Lett 36:L15812. https://doi.org/10.1029/2009GL038748

Gurubaran S, Rajaram R, Nakamura T, Tsuda T (2005) Interannual variability of diurnal tides in the tropical mesopause region: a signature of the El *Niño*-Southern Oscillation (ENSO). Geophys Res Lett 32:L13805. https://doi.org/10.1029/2005GL022928

Hagan ME, Roble RG, Hackney J (2001) Migrating thermospheric tides. J Geophys Res 106(A7):12739–12752. https://doi.org/10.1029/2000JA000344

Hagan ME, Maute A, Roble RG (2009) Tropospheric tidal effects on the middle and upper atmosphere. J Geophys Res 114:A01302. https://doi.org/10.1029/2008JA013637

Johnson NC (2013) How many ENSO flavors can we distinguish? J Clim 26:4816–4827. https://doi.org/10.1175/JCLI-D-12-00649.1

Lieberman RS, Riggin DM, Ortland DA, Nesbitt SW, Vincent RA (2007) Variability of mesospheric diurnal tides and tropospheric diurnal heating during 1997–1998. J Geophys Res 112:D20110. https://doi.org/10.1029/2007JD008578

Lin CH, Wang W, Hagan ME, Hsiao CC, Immel TJ, Hsu ML, Liu JY, Paxton LJ, Fang TW, Liu CH (2007) Plausible effect of atmospheric tides on the equatorial ionosphere observed by the FORMOSAT-3/COSMIC: three-dimensional electron density structures. Geophys Res Lett 34:L11112. https://doi.org/10.1029/2007GL029265

Lin CH, Lin JT, Chang LC, Liu JY, Chen CH, Chen WH, Huang HH, Liu CH (2012) Observations of global ionospheric responses to the 2009 stratospheric sudden warming event by FORMOSAT-3/COSMIC. J Geophys Res 117:A06323. https://doi.org/10.1029/2011JA017230

Liu H (2016) Thermospheric inter-annual variability and its potential connection to ENSO and stratospheric QBO. Earth Planets Space. https://doi.org/10.1186/s40623-016-0455-8

Liu JY, Lin CY, Lin CH, Tsai HF, Solomon SC, Sun YY, Lee IT, Schreiner WS, Kuo YH (2010) Artificial plasma cave in the low-latitude ionosphere results from the radio occultation inversion of the FORMOSAT-3/COSMIC. J Geophys Res 115:A07319. https://doi.org/10.1029/2009JA015079

Liu H, Sun Y, Miyoshi Y, Jin H (2017) ENSO effects on MLT diurnal tides: a 21 year reanalysis data-driven GAIA model simulation. J Geophys Res. https://doi.org/10.1002/2017ja024011

Lühr H, Häusler K, Stolle C (2007) Longitudinal variation of *F* region electron density and thermospheric zonal wind caused by atmospheric tides. Geophys Res Lett 34:L16102. https://doi.org/10.1029/2007GL030639

Maruyama N, Sun YY, Richards PG, Middlecoff J, Fang TW, Fuller-Rowell TJ, Akmaev RA, Liu JY, Valladares C (2016) A new source of the midlatitude ionospheric peak density structure revealed by a new Ionosphere-Plasmasphere model. Geophys Res Lett 43:2429–2435. https://doi.org/10.1002/2015GL067312

Oberheide J, Forbes JM (2008) Tidal propagation of deep tropical cloud signatures into the thermosphere from TIMED observations. Geophys Res Lett 35:L04816. https://doi.org/10.1029/2007GL032397

Oberheide J, Forbes JM, Häusler K, Wu Q, Bruinsma SL (2009) Tropospheric tides from 80 to 400 km: propagation, interannual variability, and solar cycle effects. J Geophys Res 114:D00I05. https://doi.org/10.1029/2009jd012388

Pancheva D, Mukhtarov P (2012) Global response of the ionosphere to atmospheric tides forced from below: recent progress based on satellite measurements. Space Sci Rev 161:1–35. https://doi.org/10.1007/s11214-011-9837-1

Pedatella NM, Forbes JM (2009) Interannual variability in the longitudinal structure of the low-latitude ionosphere due to the El Niño-Southern Oscillation. J Geophys Res 114:A12316. https://doi.org/10.1029/2009JA014494

Pedatella NM, Liu HL (2012) Tidal variability in the mesosphere and lower thermosphere due to the El Niño-Southern Oscillation. Geophys Res Lett 39:L19802. https://doi.org/10.1029/2012GL053383

Pedatella NM, Liu HL (2013) Influence of the El Niño Southern Oscillation on the middle and upper atmosphere. J Geophys Res Space Phys 118:2744–2755. https://doi.org/10.1002/jgra.50286

Pedatella NM, Hagan ME, Maute A (2012) The comparative importance of DE3, SE2, and SPW4 on the generation of wavenumber-4 longitude structures in the low-latitude ionosphere during September equinox. Geophys Res Lett 39:L19108. https://doi.org/10.1029/2012GL053643

Sun YY, Liu H, Miyoshi Y, Liu L, Chang LC (2018) El Niño-Southern Oscillation effect on quasi-biennial oscillations of temperature diurnal tides in the mesosphere and lower thermosphere. Earth Planets Space. https://doi.org/10.1186/s40623-018-0832-6

Taguchi M (2010) Observed connection of the stratospheric quasi-biennial oscillation with El Niño-Southern Oscillation in radiosonde data. J Geophys Res 115:D18120. https://doi.org/10.1029/2010JD014325

Torrence C, Compo GP (1998) A practical guide to wavelet analysis. Bull Am Meteorol Soc 79(1):61–78. https://doi.org/10.1175/1520-0477(1998)079%3c0061:APGTWA%3e2.0.CO;2

Wan W, Xiong J, Ren Z, Liu L, Zhang ML, Ding F, Ning B, Zhao B, Yue X (2010) Correlation between the ionospheric WN4 signature and the upper atmospheric DE3 tide. J Geophys Res 115:A11303. https://doi.org/10.1029/2010JA015527

Wang JC, Tsai-Lin R, Chang LC, Wu Q, Lin CCH, Yue J (2018) Modeling study of the ionospheric responses to the quasi-biennial oscillations of the sun and stratosphere. J Atmos Sol-Terr Phys. https://doi.org/10.1016/j.jastp.2017.07.024

Warner K, Oberheide J (2014) Nonmigrating tidal heating and MLT tidal wind variability due to the El Niño-Southern Oscillation. J Geophys Res Atmos 119:1249–1265. https://doi.org/10.1002/2013JD020407

Wu DL, Hays PB, Wilbert RS (1995) A least-squares method for spectral-analysis of space-time series. J Atmos Sci 52(20):3501–3511. https://doi.org/10.1175/1520-0469(1995)052%3c3501:ALSMFS%3e2.0.CO;2

Wu Q, Ortland DA, Killeen TL, Roble RG, Hagan ME, Liu HL, Solomon SC, Xu J, Skinner WR, Niciejewski RJ (2008a) Global distribution and interannual variations of mesospheric and lower thermospheric neutral wind diurnal tide: 1. Migrating tide. J Geophys Res 113(A5):A05308. https://doi.org/10.1029/2007JA012542

Wu Q, Ortland DA, Killeen TL, Roble RG, Hagan ME, Liu HL, Solomon SC, Xu J, Skinner WR, Niciejewski RJ (2008b) Global distribution and interannual variations of mesospheric and lower thermospheric neutral wind diurnal tide: 2. Nonmigrating tide. J Geophys Res 113(A5):A05309. https://doi.org/10.1029/2007JA012543

Xu J, Smith AK, Liu HL, Yuan W, Wu Q, Jiang G, Mlynczak MG, Russell JM III, Franke SJ (2009) Seasonal and quasi-biennial variations in the migrating diurnal tide observed by Thermosphere, Ionosphere, Mesosphere, Energetics and Dynamics (TIMED). J Geophys Res 114:D13107. https://doi.org/10.1029/2008JD011298

Yue X, Schreiner WS, Lei J, Sokolovskiy SV, Rocken C, Hunt DC, Kuo YH (2010) Error analysis of Abel retrieved electron density profiles from radio-occultation measurements. Ann Geophys 28:217–222. https://doi.org/10.5194/angeo-28-217-2010

Tang W, Xue X-H, Lei J, Dou X-K (2014) Ionospheric quasi-biennial oscillation in global TEC observations. J Atmos Solar Terr Phy 107:36–41. https://doi.org/10.1016/j.jastp.2013.11.002